Article ID:1004-4213(2011)04-0627-9

Effect of Spatial Coherence and in Incident X-ray Photon Energies on Clinical X-ray In-line Phase-contrast Imaging

XIA Tian[a,b], ZHANG Xue-long[a], MA Jun-shan[a],
CHENG Jing-hai[b], HUANG Yong[b]

(a. *School of Optical-electrical and Computer Engineering*; b. *Shanghai Medical Instrumentation College*, *University of Shanghai for Science and Technology*, *Shanghai* 200093, *China*)

Abstract: X-ray source is usually considered as a monochromatic point source, regardless of whose size effect. However, in clinical practical applications, an X-ray tube is a polychromatic source with a finite focal spot. The incident X-ray source was supposed as the average intensity distribution of a qusi-monochromatic light circular source in the beginning, and then it was extended to the polychromatic case. Based on Fresnel-Kirchhoff diffraction theory, taking the spatial coherence into account, the new in-line X-ray Phase-contrast imaging formula was derived by Fourier transform. The absorption contrast transmission function γ_{re} and phase contrast transmission function $\gamma_{re}2\pi\lambda R_2u^2/M$ were obtained from the new formula, which represented absorption effect and phase effect, respectively. The curves of the above functions for different radiuses were given by software Matlab and the optimal positions for different source radiuses were also calculated. The theoretical analysis results are as follows: 1) the spatial coherence effect should be considered when source radius is bigger enough, and decreasing the source radius would increase phase effect; 2) there is the definitive relationship between the radius and the optimal imaging position, which has been presented in a special case;3) the effect of source size on phase effect is not infinite, which could be ignored when the size is equal to a suitable value. The suitable radius is given in a special case; 4) decreasing incident X-ray photon energies would strengthen PE obviously, and the variation of photon energies has no effect on the optimal imaging position; as a result, the new formula could be extended to the polychromatic case. In order to verify the theoretical results, the micro-focus X-ray phase-contrast imaging experiments for the breakage surface of optical glass detection were carried out. Some experimental results are in good agreement with theoretical analysis, while some do not meet our expectations. The related explanations were also presented.

Key words: Phase-contrast imaging; Absorption contrast transmission function; Phase contrast transmission function

CLCN: R319; R445.9; O434.1 **Document Code**: A

doi: 10.3788/gzxb20114004.0627

0 Introduction

It is well known that conventional X-ray imaging has been used in diagnostic imaging since the X-ray was discovered by Roentgen in 1895. The X-ray was always based on the biological tissue′s different X-ray attenuation in the object caused by its varying composition, thickness or density. However, owing to the unapparent differences in X-ray absorption for soft tissues, conventional X-ray imaging would be out of use obviously. In fact, X-rays, as electromagnetic

Foundation item: Shanghai Key Discipline Fund (No. P0502), Shanghai Scientific and Technological Development Fund (No. 07ZZ93), Shanghai Major Research projects Fund (No. 06DZ11311), Shanghai Science and Technology Special Project of Talent Program Topics (No. 09QT1405900), and Shanghai Universities Select And Train Outstanding Young Teachers In Special Fund (No. slg08044)

First author: XIA Tian(1982-), male, lecture, research interests: Biomedical Optics. Email: hahasummer007@sina.com

Corresponding author: ZHANG Xue-long(19-), male, professor, research interests: Biomedical Optics. Email: xuelongz@yahoo.com.cn

Received date: 2010-10-08 **Revised date**: 2010-11-24

wave, X-ray-tissue interaction causes phase change as well when the beam passes through material such as soft tissue. As a new area of X-ray study, based on the phase change effect on the X-ray intensity image[1], X-ray phase contrast imaging (X-PCI) involves a major conceptual and practical advance in the use of X-ray imaging.

Several research groups have been hammering at exploring ways of X-PCI in the world since the 90s in the 20th century. Generally, these approaches fall into three categories on principles: interferometry[2-4], diffractometry[5-8], and in-line phase-contrast imaging[9-13]. Since the in-line phase-contrast imaging is comparatively simple and easier to be carried out, it has great potential for clinical imaging application.

In clinical applications, an X-ray tube is a polychromatic source with a finite focal spot. In order to simplify discussion, the incident X-ray source in this paper is supposed as qusi-monochromatic light in the beginning, and it is going to be extended to the case of polychromatic in the end. Moreover, the size of the focal spot discussed in this paper is very small (about 0.5～50 μm). Hence, it is assumed that the intensity of the incident X-ray source is approximately circular and uniformly distributed. On the basis of these hypotheses, the analysis of the effect of spatial coherence on clinical X-ray in-line phase-contrast imaging is presented in detail. According to the results of the analysis, the conclusion gained are as follows: 1) the spatial coherence should be considered, and decreasing the source radius would increase phase effect (PE); 2) there is the definitive relationship between the radius and the optimal imaging position, which is presented; 3) the effect of source size on PE is not infinite, which could be ignored when the size is small enough. The suitable radius is also given in a special case; 4) the variation of photon energies has no effect on the optimal imaging position, as a result, the new formula could be extended to the polychromatic case.

1 Theorectical formulas

The amount of the phase change is determined by biological tissue dielectric susceptibility, or equivalently, by the refractive index of the tissue[9]. The refractive index n for an X-ray is complex and equal to [14]

$$n=1-\delta+\mathrm{i}\beta \tag{1}$$

where δ is the refractive index decrements, and is responsible for X-ray phase shift and β is responsible for X-ray attenuation. The δ is given by references[15] and[16]

$$\delta=\left(\frac{r_e\lambda^2}{2\pi}\right)\sum_k N_k(Z_k+f_k^r)$$

where r_e, λ, N_k, Z_k and f_k^r are the classical electron radius, vacuum wavelength of incident light, atomic density, atomic number and real part of the anomalous atomic scattering factor of the element k, respectively. When the incident X-ray photon energy is away from binding energy, the above formula could be reduced to[9]

$$\delta\cong 4.49\times10^{-16}\lambda^2 N_e \tag{2}$$

where N_e is the electron density. It is found out that for infiltrating ductal carcinoma (IDC) in breast, the cancer tissue's $\delta(10^{-6}\sim10^{-8})$ is about 1000 times greater than $\beta(10^{-9}\sim10^{-11})$ for X-ray at 10～100 keV range[14].

In terms of δ, the amount of X-ray phase change from biological tissue can be calculated as[14]

$$\varphi=-\frac{2\pi}{\lambda}\int\delta(s)\mathrm{d}s \tag{3}$$

where the integral is over the ray path.

In reference[1], Pogany, Gao, and Winkins (PGW) modeled the phase shift and attenuation effects of a piece of biological tissue as a two-dimensional transmission function $T(\eta,\xi)$ at a location (η,ξ) on the object plan perpendicular to the X-ray projection direction (z axis)

$$T(\eta,\xi)=\exp\left[\mathrm{i}\varphi(\eta,\xi)-\frac{\mu(\eta,\xi)}{2}\right]=A(\eta,\xi)\mathrm{e}^{\mathrm{i}\varphi(\eta,\xi)} \tag{4}$$

where $\varphi(\eta,\xi)$ and $\mu(\eta,\xi)$ are the z projection of object phase and linear attenuation coefficients. In Eq.(4), $A(\eta,\xi)$ represents the X-ray amplitude transmission. The concrete expressions of $\varphi(\eta,\xi)$ and $\mu(\eta,\xi)$ are

$$\varphi(\eta,\xi)=-\frac{2\pi}{\lambda}\int\delta(\eta,\xi,z)\mathrm{d}z,$$

and

$$\mu(\eta,\xi)=\frac{4\pi}{\lambda}\int\beta(\eta,\xi,z)\mathrm{d}z \tag{5}$$

respectively.

Here for calculation convenience but without loss of generality, $T(\eta,\xi)$ is considered as 1-dimension form $T(\eta)$, which is the same as reference [1]. Applying the paraxial Fresnel diffraction theory to the point source geometry, the diffracted spherical X-ray wave field function arriving at a location (x,y) on the detector plane is written as[17]

$$E(x,y)=\frac{\sqrt{R_1 I_{10}}}{\sqrt{\mathrm{i}\lambda R_2(R_1+R_2)}}\exp\left(\mathrm{i}\pi\frac{2(R_1+R_2)^2+y^2}{\lambda(R_1+R_2)}\right)\cdot \int_{-\infty}^{\infty}\left\{\exp\left[\mathrm{i}\frac{\pi}{\lambda}\left(\frac{\eta^2}{R_1}+\frac{(\eta-x)^2}{R_2}\right)\right]T(\eta)\right\}\mathrm{d}\eta \quad (6)$$

where R_1 denotes the distance from the source to the object plane and R_2 denotes the distance from the object plane to the detector plane. According to the relationship between the wave field function and the intensity image, the X-ray intensity image $I(x)$ on the detector plane is

$$I(x)=E(x,y)\cdot E^*(x,y)=\frac{I_{10}}{\lambda M R_2}\cdot \int_{-\infty}^{\infty}\int_{-\infty}^{\infty}\exp\left[\mathrm{i}\pi M\frac{(\eta_1-\frac{x}{M})^2-(\eta_2-\frac{x}{M})^2}{\lambda R_2}\right]\cdot T(\eta_1)T^*(\eta_2)\mathrm{d}\eta_1\mathrm{d}\eta_2 \quad (7)$$

where I_{10} denotes the incident X-ray intensity on the object plane at R_1 and the geometric magnification factor $M=(R_1+R_2)/R_1$. Obviously, Eq. (7) is hard to be carried out. However, trying to utilize the Fourier Transform (FT) to Eq. (6) to see how the spatial frequency information of object attenuation and phase are transferred to the detector plane is necessary. The FT of the intensity is written as

$$\tilde{I}(u)=\int_{-\infty}^{\infty}[\exp(\mathrm{i}2\pi\frac{x}{M}u)\ I(x)]\mathrm{d}(\frac{x}{M}) \quad (8)$$

Substituting Eq. (7) into Eq. (8), after a tedious calculation

$$\tilde{I}(u)=\frac{I_{10}}{M^2}\exp(\frac{\mathrm{i}\pi\lambda R_2 u^2}{M})\{\mathrm{FT}[A^2(\eta)]+\frac{2\pi\lambda R_2 u^2}{M}\times\mathrm{FT}[A^2(\eta)\varphi(\eta)]+\frac{\lambda R_2 u}{M}\mathrm{FT}[A(\eta)\cdot\frac{\mathrm{d}A(\eta)}{\mathrm{d}\eta}]-2\mathrm{i}\frac{\lambda R_2 u}{M}\mathrm{FT}[A(\eta)\frac{\mathrm{d}A(\eta)}{\mathrm{d}\eta}\varphi(\eta)]\} \quad (9)$$

Eq. (8) is a generalized imaging formula with respect to spatial resolution u. It has been established that the amplitude approximation and moderate variation condition for phase can be applied to the clinical imaging in references [9], [12] and [13]. Therefore, taking the above conditions into account, Eq. (9) could be simplified as[12-13]

$$\tilde{I}(u)=\frac{I_{10}}{M^2}\cos(\frac{\pi\lambda R_2 u^2}{M})\{\mathrm{FT}[A^2(x)]+\frac{2\pi\lambda R_2 u^2}{M}\mathrm{FT}[A^2(x)\varphi(x)]\} \quad (10)$$

However, the applicability of the formula above is very limited. It is valid only for the X-ray spot light, viz. the value of spatial coherence equals to 1. Actually, the X-ray source in clinical imaging should not be regarded as a spot, whose size effect on the imaging could not be ignored. For an X-ray tube with a focal aperture of radius a, the diffraction waves generated by tissue from individual spherical waves emitted by different points of the focal spot should destruct the interference effects and the diffraction patterns could blur each other[11]. Consequently, the effect of spatial coherence is necessary to be taken into account for factual X-ray source in clinical imaging application.

In X-ray diagnostic imaging, the energy of X-ray photons ranges from 10 keV to150 keV, and the corresponding X-ray wavelength varies from 0.124 nm to 0.008 3 nm. The distance from object to detector is less than 1m in general and the maximum spatial resolution needed should be about 20 lp/mm[11]. As a result, $\pi\lambda z u^2\ll 1$, hence $\cos(\pi\lambda z u^2)\approx 1$, Eq. (10) becomes

$$\tilde{I}(u)\approx\frac{I_{10}}{M^2}\{\mathrm{FT}[A^2(x)]+\frac{2\pi\lambda R_2 u^2}{M}\cdot \mathrm{FT}[A^2(x)\varphi(x)]\} \quad (11)$$

Based on the properties of linear imaging system[11, 19-20], the reduced complex coherence degree utilized to represent the partial coherence is brought into the imaging formula.

The complex coherence degree (CCD) γ can be written as the following form according to Van Citter-Zernike theorem[17-18]

$$\gamma(P_1,P_2)=\frac{\iint I(X,Y)\exp(-\mathrm{i}\bar{k}(pX+qY))\mathrm{d}X\mathrm{d}Y}{\iint I(X,Y)\mathrm{d}X\mathrm{d}Y}\cdot \exp(\mathrm{i}\varphi) \quad (12)$$

which describes the correlation of light vibration between point $P_1(\eta_1,\xi_1)$ and point $P_2(\eta_2,\xi_2)$ on the object plane. As well known, the van Citter-Zernike theorem states that the spatial coherence function is determined by Fourier transform of the source intensity distribution over the source-point positions[17]. Here X and Y represents the coordinates on the source plane, $\bar{k}$ denotes wave vector, and $p=(\eta_1-\eta_2)/R_1$, $q=(\xi_1-\xi_2)/R_1$. Note that φ is the phase difference between P_1 and P_2, and $\varphi=\bar{k}[(\eta_1^2+\xi_1^2)-(\eta_2^2+\xi_2^2)]/2R_1$.

As mentioned above, it has been made assumption that the intensity $I(X,Y)$ on source plane is approximately circular and evenly distributed. Hence, it can be obtained

$$\gamma(r_1,r_2)=\frac{2\mathrm{J}_1(V)}{V}\exp(\mathrm{i}\varphi) \quad (13)$$

where $V=\bar{k}a\sqrt{p^2+q^2}$, a denotes the radius of the X-ray source, and $\mathrm{J}_1(V)$ denotes the one order Bessel function of the fist kind. According to the upper assumption, the object plane has been

considered as 1-dimension case in order to facilitate the calculation. Hence, $V=\bar{k}a\,|(\eta_1-\eta_2)/R_1|$. The relation that $|\eta_1-\eta_2|=\bar{\lambda}R_2u/M$ had been deduced in references[13] and[19]. Substituting the relation to Eq. (13), the reduced complex coherence degree(RCCD)can be obtained

$$\gamma_{re}(u,R_1,R_2,a)=\left|\frac{2J_1(\frac{2\pi aR_2u}{R_1M})}{\frac{2\pi aR_2u}{R_1M}}\right| \tag{14}$$

which represents the strength of the X-ray source coherence, and $0\leqslant\gamma_{re}\leqslant 1$.

Therefore, taking the effect of spatial coherence into account, the clinical X-ray imaging formula can be written as

$$\tilde{I}(u)\approx\frac{I_{10}}{M^2}\{\gamma_{re}\mathrm{FT}[A^2(x)]+\gamma_{re}\frac{2\pi\lambda R_2u^2}{M}\cdot \mathrm{FT}[A^2(x)\varphi(x)]\} \tag{15}$$

In Eq. (15), the first term and the second term are defined as the attenuation term and the phase term respectively. Correspondingly, γ_{re} can be named as Absorption Contrast Transmission Function (ACTF), and $\gamma_{re}\ 2\pi\lambda R_2u^2/M$ can be named as Phase Contrast Transmission Function (PCTF). ACTF and PCTF represent attenuation effect AE and PE, respectively. Obviously, the more values of ACTF and PCTF are, the more the strength of absorption effect (AE) and PE manifests. Enhancing the strength of PE as much as possible is an important goal in the clinical X-PCI.

While PCTF with respect to R_2 reaches the maximum, the relation can be obtained immediately

$$\frac{\partial\mathrm{PCTF}(u,R_1,R_2,a)}{\partial R_2}=0 \tag{16}$$

If the parameters of u, R_1, and a are set, the value of R_2(Viz. the optimal imaging position R_2) could be figured out. For the convenience in the following expression, the optimal imaging position R_2 for the maximal PCTF is written as R_{PCTF}.

2 Effects of source radius on AE and PE

The curves of ACTF and PCTF for different radiuses a would be provided in the section. In mammography the average X-ray photon energy is about 20 keV; let the source-detector distance (SDD) be 0.4m, hence, R_1 could be written as the relation with respect to R_2, viz. $R_1=0.4-R_2$, and the spatial resolution u of the detector is 20 lp/mm.

With the above given parameters, the curves of ACTF and PCTF with regard to R_2 for the different source radiuses ($a=0.5,1,20,50$ μm) are drawn in Fig. 1 and Fig. 2, respectively.

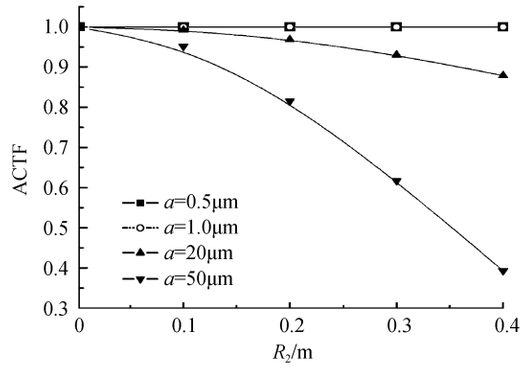

Fig. 1 The curves of attenuation-contrast transmission function for the different source radiuses

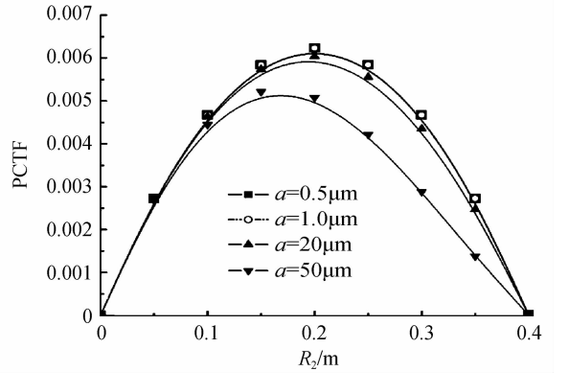

Fig. 2 The curves of phase-contrast transmission function for the different source radiuses

In Fig. 2, R_{PCTF} approaches to the half of SDD (Viz. 0.2m) when the source radius is small enough, and, it will be no more than SDD/2. Hence, $2\pi aR_2u/R_1M=2\pi aR_2u<\pi$ (the maximal calculated radius, viz. $a=50$ μm). According to Bessel function regularities of distribution, it can be obtained that $\frac{2J_1(2\pi aR_2u/R_1M)}{2\pi aR_2u/R_1M}>0$. Therefore, the formula used to figure R_{PCTF} out can be obtained from Eq. (14), Eq. (15) and Eq. (16)

$$\lambda u\{J_1(2\pi auR_{PCTF})-2\pi au(0.4-R_{PCTF})\cdot J_1'(2\pi auR_{PCTF})\}=0$$

or

$$J_1(2\pi auR_{PCTF})-\pi au(0.4-R_{PCTF})\cdot[J_0(2\pi auR_{PCTF})-J_2(2\pi auR_{PCTF})]=0 \tag{17}$$

Where J_0 and J_2 represent zero and two-order Bessel function, respectively. When $u=20$ lp/mm, the values of R_{PCTF} for different source radiuses are shown in Table 1. For $a=1$ μm, $R_{PCTF}\approx 0.199\ 9$ m≈SDD/2, which is in agreement with the conclusion in reference[12].

Table 1　The data sheet of R_{PCTF}, R_1 and M for the different source radiuses

a/μm	0.05	0.5	1	2	20	30	40	50
R_{PCTF}/m)	0.200 000	0.200 000	0.199 984	0.199 937	0.193 823	0.186 525	0.177 145	0.166 494
R_1/m	0.200 000	0.200 000	0.200 016	0.200 063	0.206 177	0.213 475	0.222 855	0.233 506
M	2	2	1.999 84	1.999 37	1.940 08	1.873 76	1.794 89	1.713 02

From Fig. 1 it can be easily seen that ACTF (viz. AE) generally decreases as R_2 increases. Furthermore, the less the radius is, the less the decrescent extent of ACTF vs R_2 is. For example, as $a=1$ μm, the difference between the maximal ACTF at $R_2=0$ and the minimal ACTF at $R_2=0.4$ m is almost equal to zero, which shows that the variation of AE vs R_2 could be neglected when the size of X-ray source is small enough. When $R_2=0$, it could be obtained that the second term in Eq. (15) is going to be zero. In that case, PE is zero and only AE left, which is in agreement with the actual case. Obviously, the value of ACTF for the smaller X-ray source is more than the one for the bigger source at the same R_2, which means that decreasing the size of X-ray source will strengthen AE. Therefore, reducing the size of X-ray source will strengthen spatial coherence and strengthen AE as well at the same time. The above analysis results show that the size for X-PCI need not to be reduced unboundedly but to be a right value, about which will be made further discussion in the following part .

From both Fig. 2 and Table. 1, it could be seen that as the size of the X-ray source increases, R_{PCTF} for the maximal PE decreases, which indicates that the optimal X-PCI position for different source radius is different, which could be calculated by Eq. (17). In clinical case, the thickness of human body must be considered, not as a plane. As a result, the optimal X-PCI position is not a value but a range. With $a=20$ μm and the body thickness of 0.1m, the optimal X-PCI position range from Fig. 2 is 0.15～0.25 m, which should be useful for the experiment designation and clinical application. Moreover, as the radius decreases, the X-ray source size contribution to PE is less and less, obviously. It is easy to be found that there is nearly no difference of the curves of PCTF when $a=1$ μm and $a=0.5$ μm in Fig. 2, which means that the variation of X-ray source size effect on PE could be ignored when the size approaches to a right value. As is well known, reducing the size of source is very hard in techniques, fortunately, the foregoing conclusion tells us that the size is not necessarily reduced unboundedly but should be a right value. From the above calculated results in Table 1, when $a=2$ μm, the radius need not be reduced any more in the case of $R_1+R_2=0.4$ m.

3　The effects of incident photon energy on PE

With the parameters of $a=1$ μm, $R_1+R_2=0.4$ m, and $u=20$ lp/mm, the curves of PCTF for different photon energies ($E=10$, 20, 40, 150 keV) are calculated for the investigation of the effect of incident photon energy on PE in Fig. 3.

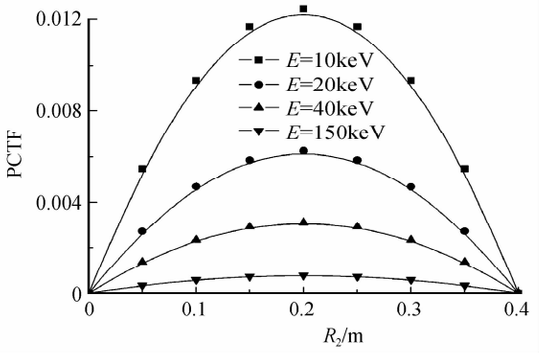

Fig. 3　The curves of phase-contrast transmission function for the different X-ray incident photon energies

It is necessary to stress that since the soft X-ray photon energies do more harm to the body, the X-ray incident photon energies discussed in this paper are all in hard X-ray rang (10～150 keV). From Fig. 3, it can be seen that the less the incident photon energy is, the more the contribution to PE it makes. Taking $E=10$ keV and $E=150$ keV for comparison, the peak value for $E=10$ keV is about 0.012, whereas the one for $E=150$ keV is about 0.001. Analyzing the curves in Fig. 3 further, when E increases from 10keV to 20 keV, correspondingly, the peak value decreases from 0.012 to 0.006, namely ΔPCTF$=0.006$; for another case, when E increases from 40 keV to 150 keV, the peak value decreases from 0.003 to 0.001, ΔPCTF$=0.002$. For easier explanation, an expression ΔPCTF/ΔE which represents the variation speed of PE with respect to E is introduced. Hence, the variation speed of PE with E for two cases could be written as 0.006/10 and 0.002/110; and then dividing the former by the latter, the result is 33, which indicates that the

effect of incident X-ray photon energies in the range from 10 keV to 20 keV manifests more sensitively than in the other range. From Eq. (2), it is fortunately found that increasing λ will both raise PCTF and the refractive index decrement δ, namely PE will be increased by two aspects.

Moreover, when the source radius is set, it is easy to obtain that from Fig. 3 there are the same value of the optimal imaging position R_2 (where the PCTF is equal to peak value) for different incident different X-ray photon energies, therefore, Eq. (16) is suitable for both the qusi-monochromatic case and the polychromatic one.

4 Experimental results

The experimental apparatus used for recording phase-contrast images is produced by YXLON International X-ray GmbH. The microfocus X-ray tube range from 10 kVp to 160 kVp, which has three modes, namely nanofocus mode ($a=0.5$ μm), microfocus mode ($a=1$ μm) and high power mode ($a>1$ μm and still in micrometer range). In high power mode, the radius of the X-ray source is larger than the other two modes due to elimination of heat. The minimal detail detectability of the detector is less than 1 μm. The distance from source to detector is 0.4 m.

The experimental sample is a natural breakage of colourless optical glass, whose material is SiO_2 ($\delta \gg \beta$ in the case of $E>10$ keV[18]). The damaged surface consists of many small anomalous steps. The minimal thickness of the step is about 0.5 mm. Due to $\delta \gg \beta$, PE is larger than AE for optical glass, and AE should be very small. Hence, the variation of received light intensity by detector is mainly determined by phase and the glass thickness change will have a direct impact on the phase change.

As is known, digital images can be expressed as $I(i,j)$, where $I(i,j)$ denotes the received light intensity by detector at the pixel location (i,j). For convenience, a method of edge detection is introduced. In the edge region, as there is a sudden change for the thickness, the light intensity will change greatly. The variable complexity of intensity gradient reflects the value of PE, and the more complex intensity gradient varies, the greater PE is. For these reasons, intensity gradient represents light intensity variation in edge region, which should be an important value for edge detection. The intensity gradient formula for digital images could be written as

$$|\nabla I(i,j)| = \{[I(i,j+1)-I(i,j-1)]^2 + [I(i+1,j)-I(i-1,j)]^2\}^{1/2} \quad (18)$$

The experimental results are shown in Fig. 4 ~ Fig. 8. Among them, the results for different light radiuses are shown from Fig. 4 to Fig. 6, the ones gained by only changing the imaging position R_2 are shown in Fig. 7, and the ones obtained by only changing the value tube voltage to gain the variation of incident light energy are also shown in Fig. 8.

4.1 Effects of light source radius on PE

It is obvious that the thickness change greatly at the edge of steps, where the phase also varies greatly. The steps could be seen clearly in the elliptic region of Fig. 4(a) and Fig. 4(b). While, the steps in Fig. 5(a) and Fig. 5(b) could not be seen clearly like in Fig. 4(a) and Fig. 4(b). The reason should be that the light source radius for nanofocus mode is half of the one for the microfocus mode, and the source area is 1/4. Therefore, the optics flux reduction caused by the diminution of light source area is visible. By comparing Fig. 4(c) with Fig. 5(c), the variation of intensity gradient in Fig. 5(c) is as complex as the one in Fig. 4(c), but the differences of adjacent

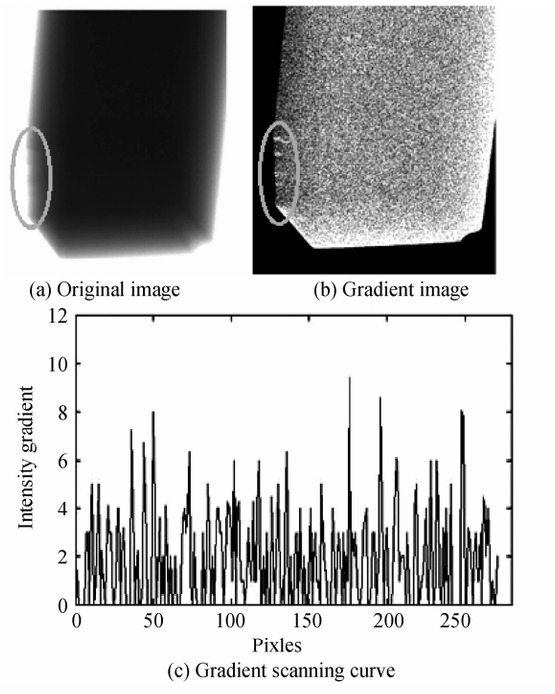

Fig. 4 (a) CCD image of damage of optical glass taken with $a=1$ μm and $R_{PCTF}=0.200\,000$ m and with the X-ray tube operating at 65 kVp and 31 μA; (b) Intensity gradient map of (a); (c) A vertical intensity gradient curve of a scanning line in the elliptic region of (b)

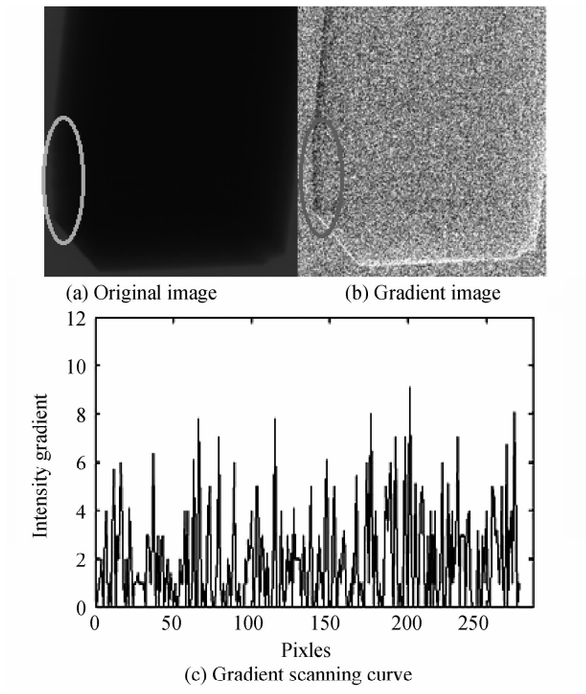

Fig. 5　(a) CCD image of damage of optical glass taken with $a=0.5$ μm and $R_{PCTF}=0.200\ 000$ m and with the X-ray tube operating at 65 kVp and 31 μA; (b) Intensity gradient map of (a); (c) A vertical intensity gradient curve of a scanning line in the elliptic region of (b)

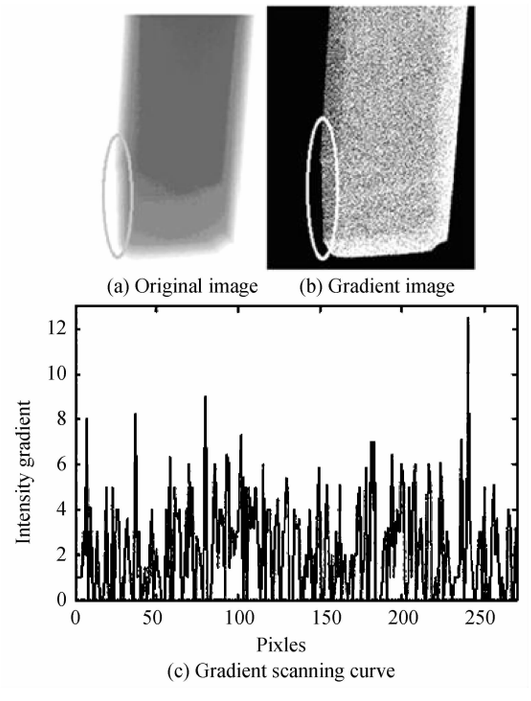

Fig. 6　(a) CCD image of damage of optical glass taken with high power mode and $R_2=0.200\ 000$ m and with the X-ray tube operating at 65 kVp and 31μA; (b) Intensity gradient map of (a); (c) A vertical intensity gradient curve of a scanning line in the elliptic region of (b)

intensity gradient in Fig. 5(c) are almost less than the ones in Fig. 4(c), which results in the imaging blurring in Fig. 5(c).

For high power mode, the source radius is bigger than the other two modes and the optics flux is large enough. However, the steps could not be seen clearly in Fig. 6(a) and there is no sharp edge in Fig. 6(b) like Fig. 4(b), which indicates that as the source size increases, the PE decreases, which agrees with the theoretical calculation.

According to the theoretical calculation and experiments, the diminution of source size could enhance PE in response, but, as the source size decrease, optics flux also weakens at the same time. As a result, the size is not necessarily reduced unboundedly but should be a right value, where PE and optics flux are both suitable. It needs further investigations of how to fix the suitable value.

4.2　Effects of R_{PCTF} on PE

In Fig. 7(a) and Fig. 7(b), the steps still could be resolved, but they are low image resolution in comparison with Fig. 4(a) and Fig. 7(a). Furthermore, from Fig. 4(c) and Fig. 7(c), it is obvious to be obtained that the variable complexity of intensity gradient in Fig. 7(c) is

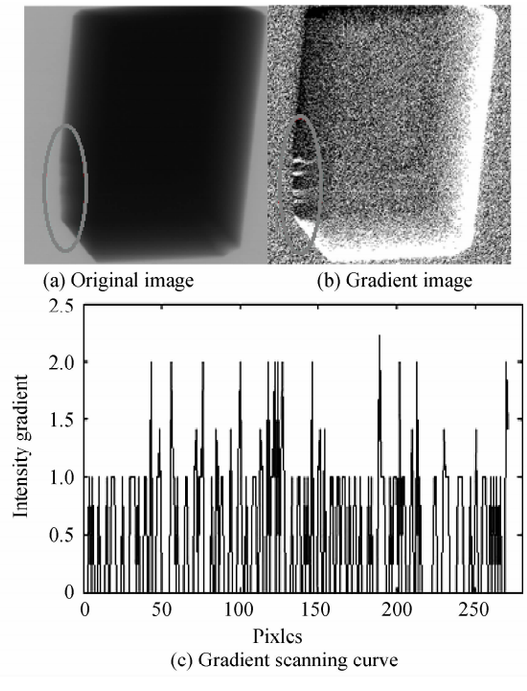

Fig. 7　(a) CCD image of damage of optical glass taken with $a=1$ μm and $R_2=0.100\ 000$ m and with the X-ray tube operating at 65 kVp and 31 μA; (b) Intensity gradient map of (a); (c) A vertical intensity gradient curve of a scanning line in the elliptic region of (b)

lower than the one in Fig. 4(c), which means that the variation of intensity caused by the change of glass thickness is detected incompletely. Moreover, the maximum of intensity gradient (less than 2.5) in Fig. 7(c) is less than the one (about 10) in Fig. 4(c). As a result, the PE will become weak when R_2 deviated from its optimal imaging position R_{PCTF}, which is very consistent with the theoretical calculation.

4.3 Effects of tube voltage on PE

As is known, the smaller tube voltage is, the greater short-wave limit is. Meanwhile, reducing tube voltage will increase the average wavelength. According to the above theoretical calculation, increasing average wavelength will enhance PE.

By comparing Fig. 8(a) with Fig. 4(a), there is no visible improvement for resolution. The complexity of variation of intensity gradient in Fig. 8(c) is not diminished in comparison with Fig. 4(c), and moreover, the maximum of intensity gradient is slightly more than the one in Fig. 4(c), but the differences of adjacent intensity gradient is significantly less than the ones in Fig. 4(c). These mean that reducing the tube voltage does not improve the resolution as we expected. The reason lies in that , reducing the voltage would make optics flux decrease at the same time. The incident light flux is not enough to let us recognize the variation of intensity.

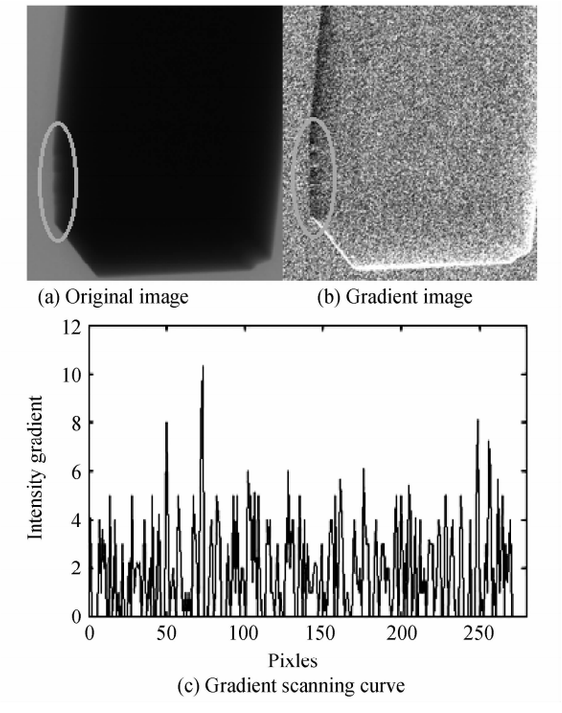

Fig. 8 (a) CCD image of damage of optical glass taken with $a=1\mu$m and $R_2=0.200\ 000$ m and with the X-ray tube operating at 50 kVp and 31 μA; (b) Intensity gradient map of (a); (c) A vertical intensity gradient curve of a scanning line in the elliptic region of (b)

5 Conclusion

The polychromatic X-ray source could be used for phase contrast imaging, which gives us hope for clinical. Polychromatic light imaging system is quite complex. A variety of factors should be considered, such as source size, tube voltage, optimal position, optics flux, which are not independent of each other. When the factors are adjusted to the suitable value, the satisfactory image could be gained. In this paper, the relationships among these factors are discussed in depth and have been given preliminary results. Further research on phase-contrast imaging will continue.

References

[1] POGANY A, GAO D, WILKINS S W. Contrast and resolution in imaging with a microfocus X-ray source[J]. *Review of Scientific Instruments*, 1997, **68**(7): 2774-2782.

[2] MOMOSE A, TAKEDA T, ITAI Y. Phase-contrast x-ray computed tomography for observing biological specimens and organic materials[J]. *Review of Scientific Instruments*, 1995, **66**(2): 1434-1436.

[3] YONEYAMA A, TAKEDA T, TSUCHIYA Y, *et al*. Coherence-contrast X-ray imaging based on X-ray interferometry[J]. *Applied Optics*, 2005, **44**(16): 3258-3261.

[4] PFEIFFER F, BUNK O, DAVID C, *et al*. High-resolution brain tumor visualization using three-dimensional X-ray phase contrast tomography[J]. *Physics in Medicine and Biology*, 2007, **52**: 6923-6930.

[5] DAVIS T J, GAO D, GUREYEV T E, *et al*. Phase contrast imaging of weakly absorbing materials using hard X-rays[J]. *Nature*, 1995, **373**(16): 595-598.

[6] KOBAYASHI K, IZUMI K, KIMURA H, *et al*. X-ray phase-contrast imaging with submicron resolution by using extremely asymmetric Bragg diffractions[J]. *Applied Physics Letters*, 2001, **78**(1): 132-134.

[7] MENK R H, RIGON L, ARFELLI F. Diffraction-enhanced X-ray medical imaging at the ELETTRA synchrotron light source[J]. *Nuclear Instruments and Methods in Physics Research Secti A*, 2005, **548**: 213-220.

[8] GUIGAY J P, PAGOT E, CLOETENS P. Fourier optics approach to X-ray analyzer-based imaging[J]. *Opt Commun*, 2007, **270**(2): 180-188.

[9] WU Xi-zeng , LIU Hong. A general theoretical formalism for X-ray phase contrast imaging[J]. *Journal of X-ray Science and Technology*, 2003, **11**(1): 33-42.

[10] GUREYEV T E, NESTERETS Y I, PAGANIN D M, *et al*. Effects of incident illumination on in-line phase-contrast imaging[J]. *JOSA A*, 2006, **23**(1): 34-42.

[11] WU Xi-zeng, LIU Hong. Clinical implementation of X-ray phase contrast imaging: theoretical foundation and design consideration[J]. *Medical Physics*, 2003, **30**(8): 2169-2179.

[12] ZHANG Xue-long, LIU Song, HUANG Yong, *et al*.

Optimal Contrast for X-ray Phase-contrast imaging. *Acta Photonica Sinica*, 2008, **37**(6): 1217-1220.

[13] XIA Tian, ZHANG Xue-long, ZHANG Guo-ying. Analysis of the absorption and the phase-effect on micro-focus X-PCI [J]. *Acta Photonica Sinica*, 2009, **38**(10): 2516-2160.

[14] WU X Z, DEAN A, LIU H. X-ray diagnostic techniques biomedical photonics handbook [M]. Tampa, FL: CRC Press, 2003: 1116.

[15] SNIGIREV A, SNIGIREVA I, KOHN V, *et al*. On the possibilities of X-ray phase contrast microimaging by coherent high-energy synchrotron radiation [J]. *Scientific Instruments*, 1995, **66**(12): 5486-5492.

[16] WILKINS S, GUREYEV T, GAO D, *et al*. Phase-contrast imaging using polychromatic hard x-rays[J]. *Nature*, 1996, **384**(28): 335-338.

[17] BORN M, WOLF E. Principles of optics: electromagnetic theory of propagation, interference and diffraction of light [M]. 7th ed. Cambridge, England: Cambridge University Press, 1999.

[18] ATTWOOD D T. Soft X-ray and extreme ultraviolet radiation: principles and application [M]. Cambridge: Cambridge University Press, 1999.

[19] WU X Z, LIU H, YAN A. Optimization of X-ray phase-contrast imaging based on in-line holography[J]. *Nuclear Instruments and Methods in Physics Research Section B*, 2005, **234**(4): 563-572.

[20] WU X Z, LIU H. An experimental method of determining relative phase- contrast factor for X-ray imaging systems[J]. *Medical Physics*, 2004, **31**: 997-1002.

空间相干与入射光子能量对临床类同轴 X 射线相衬成像影响

夏天[a,b], 张学龙[b], 马军山[a], 程敬海[b], 黄勇[b]

(上海理工大学 a. 光电学院; b. 医疗器械与食品学院, 上海 200093)

摘　要: 在临床实际应用中, X 射线源是一个具有有限尺寸的多色光源. 基于 Fresnel-Kirchhoff 衍射理论, 考虑空间相干的影响, 新的类同轴 X 射线相衬成像公式被导出. 分别代表吸收效应与相位效应的吸收衬度传递函数和相位衬度传递函数从新公式得到. 吸收衬度传递函数和相位衬度传递函数的曲线由 Matlab 给出, 不同源半径的最佳成像位置也被计算. 理论分析结果如下: 1)当光源半径足够大时空间相干效应须被考虑, 减小源半径可以增强相位效应; 2)源半径与最佳成像位置间有确定关系, 并在本文中给出; 3)源尺寸效应对相位效应影响不是无限的; 4)减小入射 X 射线光子能量将会显著增强相位效应, 但不会对最佳成像位置有影响, 因此, 上述结论可以被拓展到多色光情况. 为了验证理论结果, 本文给出了对一个表面破损的光学玻璃微聚焦相衬成像的实验结果. 其中一些实验结果与理论分析符合很好, 但也有一些实验未达到预期, 相关的解释文中也已给出.

关键词: 相衬成像, 吸收衬度传递函数, 相位衬度传递函数